

UDC 53.096:669.784

P. Bhardwaj*, S. Singh

High Pressure Research Lab., Department of Physics, Barkatullah
University, Bhopal, India
*purveebhardwaj@gmail.com

Temperature and pressure investigation of $\text{Hf}_x\text{Ta}_{1-x}\text{C}$ and $\text{Zr}_x\text{Nb}_{1-x}\text{C}$ carbide alloys

Structural mechanical and thermal properties of refractory carbides have been investigated using the Realistic Interaction Potential Approach (RIPA) model. The study has been extended to mixed crystals of $\text{Hf}_x\text{Ta}_{1-x}\text{C}$ ($0 \leq x \leq 1$) and $\text{Zr}_x\text{Nb}_{1-x}\text{C}$ ($0 \leq x \leq 1$) alloys and the effect of composition on structural and elastic properties are investigated. Phase transition pressure and associated volume collapses ($\Delta V(P_t)/V(0)$) calculated from this approach are in good agreement with available literature for the parent compounds ($x = 0$ and $x = 1$). The results for the mixed crystal counter parts are also in fair agreement with experimental data generated from the application of Vegard's law to data for the parent compounds.

Keywords: alloy, crystal structure, phase transitions, high pressure, elastic property.

INTRODUCTION

Refractory carbides are useful materials with numerous industrial applications and are of great interest to the scientific community. The industrial importance of the refractory carbides is growing rapidly, not only in the traditional and well-established applications based on the strength and refractory nature of these materials such as cutting tools and abrasives, but also in new and promising fields such as electronics and optoelectronics. The refractory carbides have been known for over one hundred years, while most of their applications are recent. These carbides have extremely high melting points. In addition to their stability these compounds are hard materials. Due to this property they are used in cutting tools, wear-resistant parts and dies. Furthermore, these refractory carbides have high electrical and thermal conductivity. These properties make these materials to be potential candidates as hard coating and thin films for electronic devices [1–3], and for a variety of high-temperature structural applications [4–7]. Among this group of carbides the four carbides: ZrC, HfC, NbC and TaC have been paid more attention in theoretical as well as experimental investigations. The melting temperature of TaC is the highest among known materials and it is about 4200 °C. Besides, these carbides are chemically very stable and have high corrosion resistance [8]. Because of these interesting properties they have potential applications in information storage technology and high power energy industry. The present carbides crystallize in simple rock-salt (B1-type) structure at normal conditions. At high pressure they transform from CsCl (B2-type) structure.

In spite of above studies [1–8] very less experimental studies have been attempted for the present refractory carbides [9, 10]. In the progression of experimental work Ihara et al. [9] have performed the X-ray photoelectron spectra

and electronic band structure of ZrC, HfC and TaC. Smith et al. [10] have studied the lattice dynamics of HfC by coherent inelastic neutron scattering. Liermann et al. [11, 12] found no phase transitions in TaC_{0.98} until 76 GPa and in NbC until 57 GPa. The X-ray diffraction patterns were recorded under pressures using synchrotron radiation. Acchar et al. [13] have studied the properties of sintered alumina reinforced with niobium carbide using X-ray diffraction. Recent electron (ESCA) and X-ray emission and absorption spectra for the cubic refractory carbides of Group IVb (TiC, ZrC, HfC) and Group Vb (VC, NbC, TaC) are summarized [14]. Based on an interpretation of the experimental data by using self-consistent-field calculations on free atoms and ions and supported by an approximately self-consistent augmented-plane-wave calculation.

Furthermore, from the theoretical point of view some studies have been reported in the literature [15–22]. Recently phase stability of various phases of MX (M = Ti, Zr; X = C, N) is examined under pressure based on first-principles calculations of the electronic and phonon structures. The results reveal that all B1 (NaCl-type) MX structures undergo a phase transition to the B2-structures under high pressure in agreement with the previous total-energy calculations by Ivashchenko et al. [15]. Amriou et al. [16] have studied electronic structure and bonding mechanism of NbC by means of accurate first principle total energy calculations using FP-LAPW. Vanderbilt et al. [17] have studied the elastic properties of cubic ZrC under high pressure by ab initio plane-wave pseudo potential density function theory (DFT) method together with local density approximation (LDA). Shrivastava et al. [18] reported the high pressure phase transitions in carbides of Ti, Hf, V, Nb and Ta by using the first principle density functional approach.

Moreover, keeping in mind various properties of present carbides like high melting point the mixed carbides show different behavior. The melting points of the mixed-metal carbides outperform those of the pure-metal carbides. The higher melting points in the mixed-metal carbides were attributed to composition changes due to the selective evaporation of carbon during melting. Mixed-metal carbides have been examined for their melting point and hot-hardness behavior as well [19]. In order to study the alloys of carbide, the first principle calculations on the electronic structure have been performed on alloys Ti_xNb_{1-x}C, Zr_xNb_{1-x}C, and Hf_xNb_{1-x}C [20]. Farkas et al. [21] investigated the thermodynamic analysis of carbide precipitates in a niobium-zirconium carbon alloy. This examination of the free energies of the formation of different carbide phases, their evolution and stability at the high temperatures, and a comparison with experimental analysis was made. Sun Xiao-Wei et al. [22] have investigated the structural, elastic, electronic, and thermodynamic properties of Zr_xNb_{1-x}C alloys using the first principles method based on the density functional theory. The modelling for transition metal compounds is not an easy task. To understand the nature of interatomic forces in the present compounds, the role of phenomenological models is significant. The phenomenological models based on various interatomic interaction energies are used to determine stable structure and mechanical properties. Furthermore, the phenomenological lattice models have been established very successful in attaining qualitative and quantitative understanding. Also the reported theoretical calculations based on the density functional theory have not considered the van-der Waals interactions. To the best of our knowledge no model calculations including temperature and covalence effect are reported for the alloy of Zr, Nb, Hf, and Ta carbides..

For the most part the available literature reports about pressure by taking temperature as $T = 0$ K. None of the studies we found about carbides addresses the progress of their structural, elastic, and thermophysical properties at high temperatures using model calculations. At the same time experimental measurements are performed at room temperature. To make the study realistic, it should be performed by taking temperature effects. To accomplish this gap we are including the role of temperature in the present investigation. It is distinguished that the refractory metal carbides are highly covalent due to the presence of two electrons in the outer most orbits. We therefore apply a Modified Interaction Potential Model, which includes the covalence and temperature effect in the potential model.

This paper supplies an inventive study of structural, mechanical, and thermal properties of ZrC, HfC, NbC, and TaC using the Realistic Interaction Potential Approach (RIPA) model. Different properties of the alloy of carbides of Zr, Nb, Hf, and Ta at room and high temperatures have been calculated successfully. In the following sections we represent the present model and calculation, the results obtained for present carbides.

PRESENT MODEL AND CALCULATION

A change in the volume of the crystal occurs after applying the pressure and it revises the charges distribution of the electron shells accordingly. Due to this reason, a deformation of the overlapping electron shells of the adjacent ions takes place which leads to an increased charge transfer (or three body interaction (TBI) [23]). This interaction becomes more important to consider due to the decrease in inter-ionic spacing of the lattice crystal when pressure gets increased and when anions experience adequate overlap.

The effect of this charge transfer is introduced in the expressions of Gibbs free energy ($G = U + pV - TS$), in order to obtain the stability condition for a crystal structure. Here, U is the internal energy, which at $T = 0$ K is equivalent to the lattice energy, p is the pressure, V is the volume, and S is the entropy.

The Gibbs free energies for rock-salt (NaCl, B1) and caesium-chloride (CsCl, B2) structures at room temperature $T = 300$ K are given by

$$G_{B1}(r) = U_{B1}(r) + pV_{B1}(r) - TS_1 ; \quad (1)$$

$$G_{B2}(r') = U_{B2}(r') + pV_{B2}(r') - TS_2 . \quad (2)$$

With $V_{B1} = 2.00r^3$ and $V_{B2} = 1.54r'^3$ as unit cell volumes S_1 and S_2 are the entropies for B1 and B2 phases, respectively. In fact the condition for a transition is that the difference in free energy between two phases should approach zero:

$$\Delta G = \Delta H - T\Delta S . \quad (3)$$

The first terms in (2) and (3) are lattice energies for B1 and B2 structures and they are expressed as

$$U_{B1}(r) = U_C(r) + U_{TBI}(r) + U_{vdW}(r) + U_{HF}(r) ; \quad (4)$$

$$U_{B2}(r') = U_C(r') + U_{TBI}(r') + U_{vdW}(r') + U_{HF}(r') . \quad (5)$$

Here U_C stands for the long range Coulomb energy, U_{TBI} for three body interactions corresponding to the nearest neighbor separation, U_{vdW} for van der Waals' interaction and U_{HF} for the energy due to the overlap repulsion represented by Hafemeister and Flygare (HF) type potential [24], and extended up to the

second neighbor ions. These contributions can be calculated using the following expressions:

for B1 structure,

$$U_C(r) = \frac{-\alpha_m z^2 e^2}{r};$$

$$U_{\text{TBI}}(r) = \frac{-12\alpha_m z e^2 f_m(r)}{r};$$

$$U_{\text{vdW}}(r) = -\left[\frac{C}{r^6} + \frac{D}{r^8}\right];$$

$$U_{\text{HF}}(r) = 6b\beta_{ij} \exp\left(\frac{r_i + r_j - r}{\rho}\right) + 6b\beta_{ii} \exp\left(\frac{2r_i - 1.414r}{\rho}\right) + 6b\beta_{jj} \exp\left(\frac{2r_j - 1.414r}{\rho}\right),$$

and for B2 structure,

$$U_C(r') = \frac{-\alpha'_m z^2 e^2}{r'};$$

$$U_{\text{TBI}}(r') = \frac{-16\alpha'_m z e^2 f_m(r')}{r'};$$

$$U_{\text{vdW}}(r') = -\left[\frac{C'}{r'^6} + \frac{D'}{r'^8}\right];$$

$$U_{\text{HF}}(r') = 8b\beta_{ij} \exp\left(\frac{r_i + r_j - r'}{\rho}\right) + 3b\beta_{ii} \exp\left(\frac{2r_i - 1.154r'}{\rho}\right) + 3b\beta_{jj} \exp\left(\frac{2r_j - 1.154r'}{\rho}\right).$$

In the above expressions α_m and α'_m are the Madelung constants for B1 and B2 structures, respectively. C (C') and D (D') are the overall van der Waals coefficients of B1 (B2) phases [25, 26], β_{ij} ($i, j = 1, 2$) are the Pauling coefficients defined as $\beta_{ij} = 1 + (Z_i/n_i) + (Z_j/n_j)$ with Z_i (Z_j), and n_i (n_j) are the valence and the number of electrons of the i (j)th ion. Ze is the ionic charge and b (ρ) are the hardness (range) parameters, r (r') are the nearest neighbor separations for B1 (B2) structure, $f_m(r)$ is the modified three body force parameter, which includes the covalency effect with three body interaction, r_i (r_j) are the ionic radii of ions i (j).

The covalency effects have been included in three-body interaction parameter in the second terms of lattice energies given by equations (1) and (2) [27, 28]. The modified three body parameter $f_m(r)$ can be obtained using the following steps:

$$f_m(r) = f_{\text{TBI}}(r) + f_{\text{cov}}(r), \quad (6)$$

where the unmodified three body parameter, $f_{\text{TBI}}(r)$, is determined by the equation

$$f_{\text{TBI}}(r) = f_0 e^{-r/\rho},$$

where f_0 is a constant. Here ρ is the range parameter. The $f(r)$ due to covalency f_{cov} is given by

$$f_{\text{cov}}(r) = \frac{4V_{sp\sigma}^2 e^2}{rE_g^3};$$

$$\frac{V_{sp\sigma}^2}{E_g^2} = \frac{1 - e_s^*}{12}; \quad (7)$$

$$E_g = E - I + \frac{(2\alpha - 1)e^2}{r}.$$

With the $V_{sp\sigma}$ as the transfer matrix between the outer most p orbital of anion and lowest excited state of cation, E_g is the transfer energy of electron from anion to cation. (In the equation of E_g , α is the ionic polarizability). By denoting the static and optical dielectric constants, ϵ_0 and ϵ , respectively and the transverse optical phonon frequency at the zone centre by ω_b , e_s represented as

$$(e_s^*)^2 = \frac{9\mu\omega_t^2(\epsilon_0 - \epsilon_\infty)}{4\pi N(\epsilon_\infty + 2)^2}$$

and (8)

$$\frac{(e_s^*)^2}{e^2} = \frac{9\nu\mu\omega_0^2(\epsilon_0 - \epsilon_\infty)}{4\pi e^2(\epsilon_\infty + 2)^2},$$

where ν denotes the unit cell volume: $2r^3$, r is the equilibrium value of the separation of the nearest neighboring ions, ϵ_0 is the static dielectric constants, μ is the reduced mass of the ions, and ω_0 is the infrared dispersion frequency.

Now the entropy differences in the last term of Eqs. (1) and (2) can be calculated from the relation used by our earlier work [29]:

$$S_1 - S_2 = \int_1^2 \left[\frac{C_1 - C_2}{T} \right], \quad (9)$$

here, 1 and 2 stands for the B1 and B2 phases, C_1 and C_2 are the specific heats of the two phases at constant pressure and their values can be calculated by the knowledge of Gruneisen parameter γ and linear isothermal temperature coefficients β as

$$C_i = \frac{\{\beta V_i B\}_i}{\gamma_i}, \quad (10)$$

here, Gruneisen parameter γ can be calculated by the well known formula as follows [28]

$$\gamma = \frac{-r_0}{6[U'''(r_0)/U''(r_0)]}. \quad (11)$$

From the knowledge of the lattice energy and the following equilibrium conditions three model parameters b (hardness), ρ (range) and $f_m(r)$ (modified three body force parameter) have been derived [27–29]

$$\left[\frac{dU}{dr} \right]_{r=r_0} = 0, \quad (12)$$

and the bulk modulus

$$B = \frac{1}{9kr_0} \left[\frac{d^2U}{dr^2} \right]_{r=r_0}, \quad (13)$$

where k is the crystal structure dependent constant and r_0 is the lattice constant.

According to the virtual crystal approximation (VCA) [30], the mixed crystals are regarded as any array of average ions whose masses, force constants, and effective charges are considered to scale linearly with concentration x . The measured

data on the lattice constants in $\text{Hf}_x\text{Ta}_{1-x}\text{C}$ and $\text{Zr}_x\text{Nb}_{1-x}\text{C}$ have shown that they vary linearly with the composition x , and hence they follow Vegard's law

$$a(A_xB_{1-x}C) = (1-x)a(AC) + xa(BC). \quad (14)$$

The values of these model parameters are the same for end point members. The values of these parameters for their mixed crystal components have been determined from the application of Vegard's law to the corresponding measured data for AC and BC . It is instructive to point that the mixed crystals, according to the virtual crystal approximation, are regarded as an array of average ions whose masses, force constants, and effective charges are considered to scale linearity with concentration. It is convenient to find the three parameters for both binary compounds. Furthermore, we assume that these parameters vary linearly with x and hence follow Vegard's law

$$b(A_xB_{1-x}C) = (1-x)b(AC) + xb(BC); \quad (15)$$

$$\rho(A_xB_{1-x}C) = (1-x)\rho(AC) + x\rho(BC); \quad (16)$$

$$f(r)(A_xB_{1-x}C) = (1-x)f(r)(AC) + xf(r)(BC). \quad (17)$$

RESULT AND DISCUSSION

Structural properties

After applying the minimization technique to $G_{B1}(r)$ and $G_{B2}(r')$, we have obtained inter ionic separations r and r' , for B1 and B2 phases, respectively at different pressures. We have evaluated the corresponding Gibbs free energy differences $\Delta G = (G_{B1}(r) - G_{B2}(r'))$. The pressure at which ΔG approaches zero is the phase transition pressure p_t . The change in minimized Gibbs free energy of both the phases has been plotted with pressure in Fig. 1 and 2 for $\text{Hf}_x\text{Ta}_{1-x}\text{C}$ and $\text{Zr}_x\text{Nb}_{1-x}\text{C}$, respectively. The plot represents the variation of Gibbs free energy change at different concentration x . We have plotted the variation of transition pressures with composition x in Fig. 3 and compared with their theoretical and pseudo-theoretical values (interpolated from the others theoretical values of the two end crystals) [31]. It is obvious from Fig. 3 that composition dependence of the transition pressure obtained presently is in close agreement with their theoretical values. The values of p_t at different compositions have been obtained from the linear interpolation

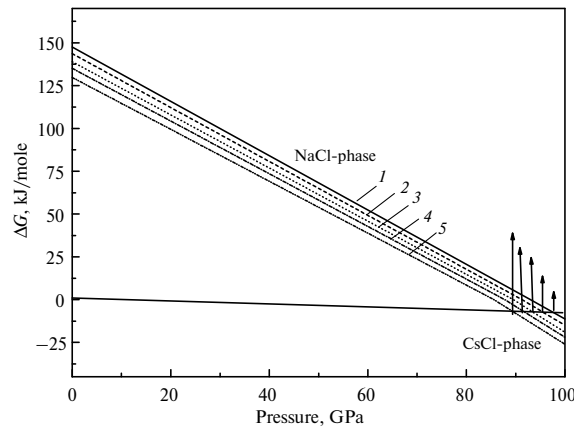


Fig. 1. Gibbs free energy with the variations of pressure for alloy $\text{Hf}_x\text{Ta}_{1-x}\text{C}$: $x = 0$ (1), 0.25 (2), 0.5 (3), 0.75 (4), 1.0 (5).

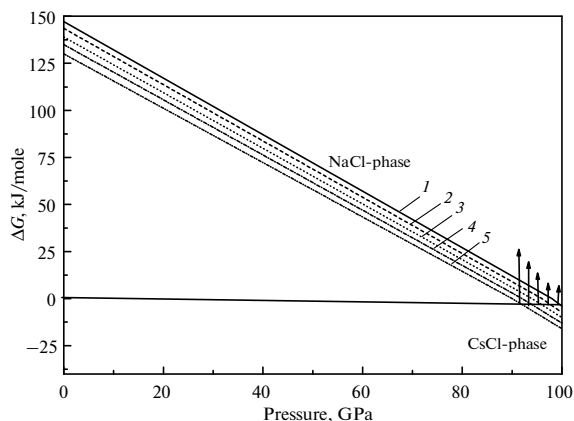


Fig. 2. Gibbs free energy with the variations of pressure for alloy $Zr_xNb_{1-x}C$: $x = 0$ (1), 0.25 (2), 0.5 (3), 0.75 (4), 1.0 (5).

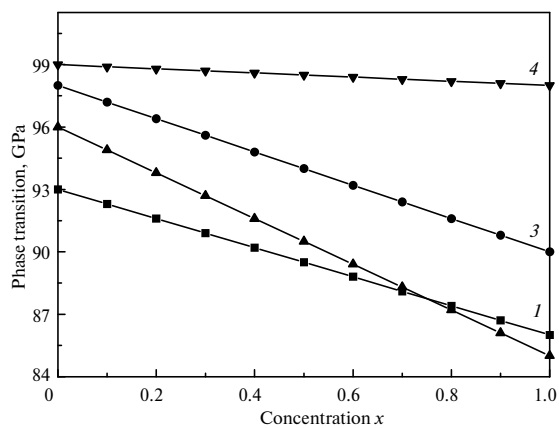


Fig. 3. Variation of phase transition with concentration x for alloys $Hf_xTa_{1-x}C$ (1, 2) and $Zr_xNb_{1-x}C$ (3, 4): present (1, 3), others (2, 4).

between the transition pressures of the two end crystals. To study the phase transition at high temperatures, we have plotted the calculated values of phase transition pressures at different temperatures in Fig. 4. It is clearly seen from this figure that there is a linear decrease of p_t occur with high temperature. So, we can decrease phase transition pressure by applying temperature.

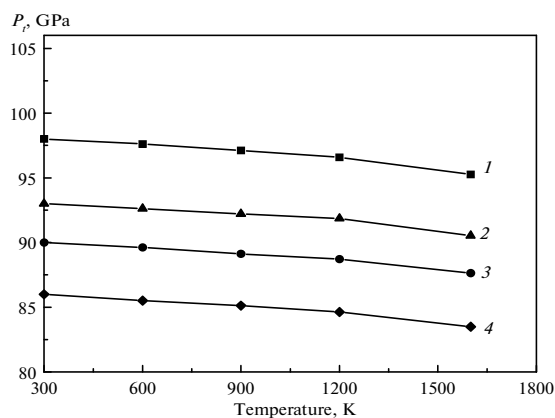


Fig. 4. Variation of phase transition with temperature for the parent compounds ZrC (1), TaC (2), NbC (3), and HfC (4).

Phase transition pressures are associated with a sudden collapse in volume. The values of relative volume have been reported in Table 1. These results have been compared with other data at different concentrations [31]. Relative volumes $\Delta V(p)/V(0)$ for different concentrations have been plotted against pressure for $\text{Hf}_x\text{Ta}_{1-x}\text{C}$ and $\text{Zr}_x\text{Nb}_{1-x}\text{C}$ in Figs. 5 and 6. The values of volume collapses $\Delta V(p_i)/V(0)$ obtained from present calculation are plotted with the variation of concentration x . At each concentration there is a sudden collapse in volume at the transition pressure.

Table 1. Phase transition and volume change of $\text{Hf}_x\text{Ta}_{1-x}\text{C}$ and $\text{Zr}_x\text{Nb}_{1-x}\text{C}$ alloys at $T = 300\text{ K}$

Alloy and concentration x	Phase transition pressure, GPa		Volume collapse, %	
	present	others	present	others
$\text{Hf}_x\text{Ta}_{1-x}\text{C}$				
0	93	96 ^a	7.8	7.6 ^a
0.25	91.25	93.25 ^{a*}	7.6	7.4 ^{a*}
0.50	89.5	90.50 ^{a*}	7.4	7.2 ^{a*}
0.75	87.75	87.75 ^{a*}	7.2	7.0 ^{a*}
1.0	86	85 ^a	7.0	6.8 ^a
$\text{Zr}_x\text{Nb}_{1-x}\text{C}$				
0	98	99 ^a	7.1	5.6 ^a
0.25	96	98.75 ^{a*}	7.625	6.45 ^{a*}
0.50	94	98.50 ^{a*}	8.15	7.30 ^{a*}
0.75	92	98.25 ^{a*}	8.675	8.15 ^{a*}
1.0	90	98 ^a	9.2	9.0 ^a

a – ref. [31], a* – pseudo-theoretical values (interpolated from the others theoretical values of the two end crystals).

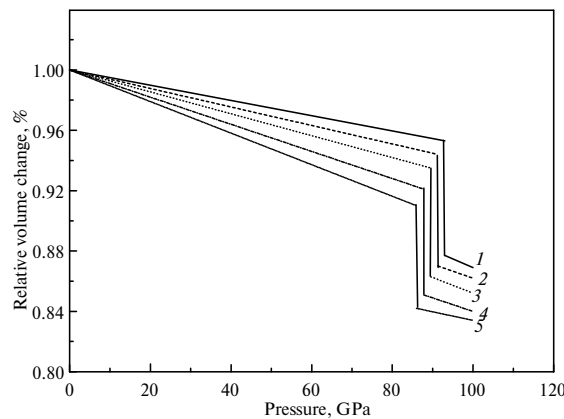


Fig. 5. Variation of relative volume (%) with pressure at different concentration x for alloy $\text{Hf}_x\text{Ta}_{1-x}\text{C}$: $x = 0$ (1), 0.25 (2), 0.5 (3), 0.75 (4), 1.0 (5).

Figures 7 and 8 show the variation of the calculated equilibrium lattice constant and as a function of concentrations x for $\text{Hf}_x\text{Ta}_{1-x}\text{C}$ and $\text{Zr}_x\text{Nb}_{1-x}\text{C}$ alloys. The obtained results for the composition dependence of the calculated equilibrium lattice parameter exhibit an agreement with experimental [32] and theoretical results [8, 33]. In going from TaC to HfC and ZrC to NbC, when the Hf and Nb content in-

creases, the values of the lattice parameters of the $\text{Hf}_x\text{Ta}_{1-x}\text{C}$ and $\text{Zr}_x\text{Nb}_{1-x}\text{C}$ alloys increase. From Table 2 and Figs. 7 and 8 our results follow the tendency demonstrated by both experimental measurement and theoretical calculations. Usually, in the treatment of alloys where the experimental data are rare, it is assumed that the atoms are located at the ideal lattice sites and the lattice constant varies linearly with concentrations x according to the Vegard's law.

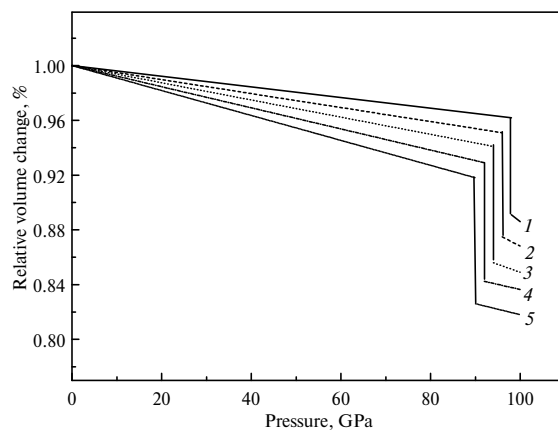


Fig. 6. Variation of relative volume (%) with pressure at different concentration x for alloy $\text{Zr}_x\text{Nb}_{1-x}\text{C}$: $x = 0$ (1), 0.25 (2), 0.5 (3), 0.75 (4), 1.0 (5).

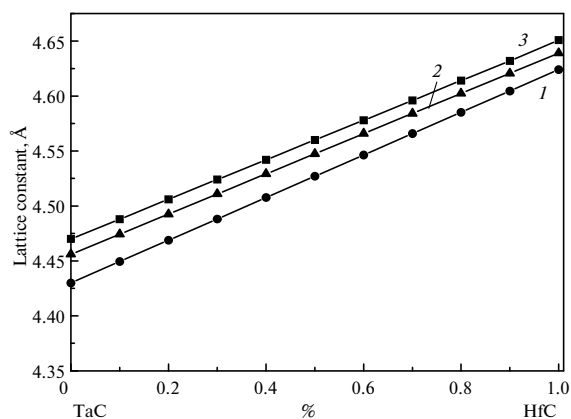


Fig. 7. Lattice constant for alloys $\text{Hf}_x\text{Ta}_{1-x}\text{C}$ with the variation of % of TaC and HfC: present (1), experiment (2), others (3).

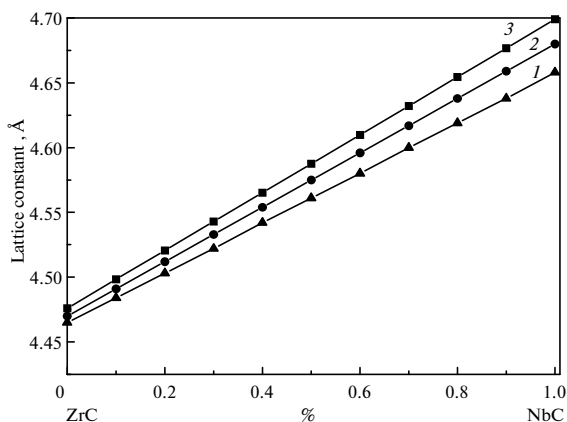


Fig. 8. Lattice constant for alloy $\text{Zr}_x\text{Nb}_{1-x}\text{C}$ with the variation of % of ZrC and NbC: present (1), experiment (2), others (3).

Table 2. Lattice constant and bulk modulus of $\text{Hf}_x\text{Ta}_{1-x}\text{C}$ and $\text{Zr}_x\text{Nb}_{1-x}\text{C}$ alloys at $T = 300 \text{ K}$

Alloy and concentration x	Lattice constant, Å			Bulk modulus, GPa		
	present	experi- ment	others	present	experi- ment	others
$\text{Hf}_x\text{Ta}_{1-x}\text{C}$						
0	4.430	4.456 ^a	4.47 ^b	326	345 ^c	324 ^b
0.25	4.478	4.501 ^{a*}	4.515 ^{b*}	304.5	324.5 ^{c*}	302.5 ^{b*}
0.50	4.527	4.547 ^{a*}	4.560 ^{b*}	283	304 ^{c*}	281 ^{b*}
0.75	4.575	4.593 ^{a*}	4.605 ^{b*}	261.5	283.5 ^{c*}	259.5 ^{b*}
1.0	4.624	4.639 ^a	4.651 ^b	240	263 ^c	238 ^b
$\text{Zr}_x\text{Nb}_{1-x}\text{C}$						
0	4.465	4.471 ^a	4.476 ^b	333.33	331	301 ^b
0.25	4.513	4.526 ^{a*}	4.531 ^{b*}	304.66	–	281.25 ^{b*}
0.50	4.561	4.581 ^{a*}	4.587 ^{b*}	275.99	–	261.5 ^{b*}
0.75	4.609	4.636 ^{a*}	4.643 ^{b*}	247.32	–	241.75 ^{b*}
1.0	4.658	4.692 ^a	4.699 ^b	218.66	–	222 ^b

a – ref. [32], b – ref. [8], c – ref. [33], a* – pseudo-theoretical values (interpolated from the other theoretical values of the two end crystals, b* and c* – pseudo-experimental values (interpolated from the other experimental values of the two end crystals).

Elastic properties

In order to calculate the modulus of elasticity for present carbides and their alloys were determined using RIPA model and application of Vegard's law. The calculated values of second order elastic constants C_{11} , C_{12} and C_{44} have been reported in Tables 3 and 4 for $\text{Hf}_x\text{Ta}_{1-x}\text{C}$ and $\text{Zr}_x\text{Nb}_{1-x}\text{C}$, respectively. At different concentrations our values have been compared with available experimental [34] and other theoretical results [22]. It is clear from both Tables that our results are in general in good agreement with available experimental results. The values we calculated are approximately in agreement with other theoretical calculations and experimental data for $x = 0$. Present approach follows the tendency demonstrated by both experimental measurement and theoretical calculations. The formulas used for calculation are given in Appendix.

The hardness of a material can be determined by using the bulk modulus. The isotropic bulk modulus of a cubic crystal is given by

$$B = \frac{C_{11} + 2C_{12}}{3}. \quad (18)$$

The calculated values of bulk modulus have been reported in Table 2 along with the comparisons with both experimental measurement and theoretical calculations at different concentrations. It is clearly seen from this Table that the value of bulk modulus linearly with concentration x . This trend shows similar behavior with others and experimental results.

The shear modulus G can be defined by the following equation:

$$G = \frac{G_V + G_R}{2}, \quad (19)$$

where $G_V = (2C + 3C_{44})/5$, $G_R = 15(6/C + 9/C_{44})^{-1}$, $C = (C_{11} - C_{12})/2$, G_V is the Voigt shear modulus and G_R is the Reuss shear modulus.

Table 3. Elastic constants C_{ij} (GPa) of $\text{Hf}_x\text{Ta}_{1-x}\text{C}$ alloys at $T = 300$ K

Concentration x	C_{11}			C_{12}		C_{44}	
	present	experiment	others	present	others	present	others
0	526	550 ^a	694 ^b	226	127 ^b	116	127 ^b
0.1	521.7	545 ^a	670.01 ^{b*}	215.3	122.95 ^{b*}	109.1	122.95 ^{b*}
0.2	517.4	540 ^a	646.02 ^{b*}	204.6	118.9 ^{b*}	102.2	118.9 ^{b*}
0.3	513.1	535 ^a	622.03 ^{b*}	193.9	114.85 ^{b*}	98.3	114.85 ^{b*}
0.4	508.8	530 ^a	598.04 ^{b*}	183.2	110.8 ^{b*}	88.4	110.8 ^{b*}
0.5	504.5	525 ^a	574.05 ^{b*}	172.5	106.75 ^{b*}	81.5	106.75 ^{b*}
0.6	500.2	520 ^a	550.06 ^{b*}	161.8	102.7 ^{b*}	74.6	102.7 ^{b*}
0.7	495.9	515 ^a	526.07 ^{b*}	151.1	98.65 ^{b*}	67.7	98.65 ^{b*}
0.8	491.6	510 ^a	502.08 ^{b*}	140.4	94.6 ^{b*}	60.8	94.6 ^{b*}
0.9	487.3	505 ^a	478.09 ^{b*}	129.7	90.55 ^{b*}	53.9	90.55 ^{b*}
1.0	483	500 ^a	454.1 ^b	119	86.5 ^b	47	86.5 ^b

a – ref. [34], b – ref. [31], a – pseudo-theoretical values (interpolated from the other theoretical values of the two end crystals), b* – pseudo-experimental values (interpolated from the other experimental values of the two end crystals).

Table 4. Elastic constants C_{ij} (GPa) of $\text{Zr}_x\text{Nb}_{1-x}\text{C}$ alloys at $T = 300$ K

Concentration x	C_{11}			C_{12}			C_{44}		
	present	experiment	others	present	experiment	others	present	experiment	others
0	614	620 ^a	667 ^b	193	200 ^a	117 ^b	146	150 ^a	168 ^b
0.1	598.8	605 ^{a*}	646 ^{b*}	183.4	190 ^{a*}	124 ^{b*}	146.5	151 ^{a*}	179 ^{b*}
0.2	583.6	590 ^{a*}	661 ^{b*}	173.8	180 ^{a*}	111 ^{b*}	147.0	152 ^{a*}	181 ^{b*}
0.3	568.4	575 ^{a*}	627 ^{b*}	164.2	170 ^{a*}	122 ^{b*}	147.5	153 ^{a*}	179 ^{b*}
0.4	553.2	560 ^{a*}	616 ^{b*}	154.6	160 ^{a*}	118 ^{b*}	148.0	154 ^{a*}	187 ^{b*}
0.5	538.0	545 ^{a*}	601 ^{b*}	145.0	150 ^{a*}	116 ^{b*}	148.5	155 ^{a*}	186 ^{b*}
0.6	522.8	530 ^{a*}	570 ^{b*}	135.4	140 ^{a*}	119 ^{b*}	149.0	156 ^{a*}	187 ^{b*}
0.7	507.6	515 ^{a*}	550 ^{b*}	125.8	130 ^{a*}	115 ^{b*}	149.5	157 ^{a*}	190 ^{b*}
0.8	492.4	500 ^{a*}	531 ^{b*}	116.2	120 ^{a*}	109 ^{b*}	150.0	158 ^{a*}	185 ^{b*}
0.9	477.2	485 ^{a*}	496 ^{b*}	106.6	110 ^{a*}	107 ^{b*}	150.5	159 ^{a*}	172 ^{b*}
1.0	462	470 ^a	458 ^b	97	100 ^a	104 ^b	151	160 ^a	152 ^b

a – ref. [34], b – ref. [22], a* – pseudo-theoretical values (interpolated from the other theoretical values of the two end crystals), b* – pseudo-experimental values (interpolated from the other experimental values of the two end crystals).

We have also calculated the Young modulus Y , which is related to the bulk modulus B and the shear modulus G by the following equation:

$$Y = 9BG(3B + G). \quad (20)$$

We have calculated the elastic anisotropic parameter and Poisson ratio σ of present compounds, using the following relations:

$$A = \frac{2C_{44}}{C_{11} - C_{12}}; \quad (21)$$

$$\sigma = \frac{3B - 2G}{6B + 2G}. \quad (22)$$

For an ideal isotropic system, A is unity and deviation from unity measures the amount of elastic anisotropy. The Young's modulus Y and Poisson's ratio σ are very important properties for industrial applications. The Young's modulus Y , the ratio of the tensile stress to the corresponding tensile strain, is required to provide information about the measure of the stiffness of the solids. All these calculated moduli are listed in Tables 5 and 6 for $\text{Hf}_x\text{Ta}_{1-x}\text{C}$ ($0 \leq x \leq 1$) and $\text{Zr}_x\text{Nb}_{1-x}\text{C}$ ($0 \leq x \leq 1$) alloys respectively. It is obvious from these Tables that when we go from TaC to HfC the values of G and Y increase with concentration while values of σ decrease with concentration. Furthermore, when we go from NbC to ZrC the values of G , Y and σ decrease with concentration.

Table 5. Shear modulus G , Young's modulus Y , and Poisson' ratio σ of $\text{Hf}_x\text{Ta}_{1-x}\text{C}$ alloy at $T = 300$ K

Concentration x	G , GPa		Y , GPa		σ	
	present		present		present	
0	129.6		343.30		0.320	
0.1	134.72		352.32		0.307	
0.2	139.84		361.34		0.294	
0.3	144.96		370.36		0.281	
0.4	150.08		379.39		0.268	
0.5	155.20		388.41		0.255	
0.6	160.32		397.43		0.242	
0.7	165.44		406.46		0.229	
0.8	170.56		415.48		0.216	
0.9	175.68		424.50		0.203	
1.0	180.8		433.53		0.190	

Table 6. Shear modulus G , Young's modulus Y and Poisson' ratio σ of $\text{Zr}_x\text{Nb}_{1-x}\text{C}$ alloy at $T = 300$ K

Concentration x	G , GPa		Y , GPa		σ	
	present	others	present	others	present	others
0	171.8	205 ^a	439.83	632 ^a	0.280	0.15 ^a
0.1	170.98	209 ^{a*}	435.12	606 ^{a*}	0.272	0.16 ^{a*}
0.2	170.16	214 ^{a*}	430.42	629 ^{a*}	0.264	0.14 ^{a*}
0.3	169.34	205 ^{a*}	425.72	587 ^{a*}	0.256	0.16 ^{a*}
0.4	168.52	210 ^{a*}	421.02	578 ^{a*}	0.248	0.16 ^{a*}
0.5	167.7	207 ^{a*}	416.32	563 ^{a*}	0.240	0.16 ^{a*}
0.6	166.88	202 ^{a*}	411.62	529 ^{a*}	0.232	0.17 ^{a*}
0.7	166.06	200 ^{a*}	406.92	510 ^{a*}	0.224	0.17 ^{a*}
0.8	165.24	195 ^{a*}	402.22	494 ^{a*}	0.216	0.17 ^{a*}
0.9	164.42	181 ^{a*}	397.52	459 ^{a*}	208	0.18 ^{a*}
1.0	163.6	162 ^a	392.82	420 ^a	0.200	0.19 ^a

a – ref. [22], a* – pseudo-theoretical values (interpolated from the others theoretical values of the two end crystals).

CONCLUSION

The structural and elastic properties of $\text{Hf}_x\text{Ta}_{1-x}\text{C}$ ($0 \leq x \leq 1$) and $\text{Zr}_x\text{Nb}_{1-x}\text{C}$ ($0 \leq x \leq 1$) alloys are systematically investigated using the virtual crystal approximation and the results are compared with experimental and theoretical results. Our calculated lattice constants of present compounds are in good agreement with the experimental data. Present Realistic Interaction Potential Approach (RIPA) model successfully studied the theoretical calculations at room temperature and not at $T = 0$ K. To obtain better theoretical results as compared with experiments we have taken here the temperature effect along with covalency effect in pressure induced theoretical calculations. Such a way, different properties of the alloy of carbides of Zr, Nb, Hf, and Ta at room and high temperatures have been calculated effectively.

Authors are thankful to Department of Science & Technology (DST), New Delhi for the financial support to this work. One of the authors (PB) is grateful to Department of Science & Technology (DST), New Delhi for, awarding WOS-‘A’ (Grant No. SR/WOS-A/PS-17/2013).

APPENDIX

The expressions for the second order elastic constants (SOECs), pressure derivatives of SOECs and third order elastic constants are expressed [29] for NaCl (B_1) as follows:

$$C_{11} = (e^2 / 4a^4)[-5.112Z(Z + 12f_m(r)) + A_1 + (A_2 + B_2) / 2 + 9.3204zaf'_m(r)]; \quad (\text{A.1})$$

$$C_{12} = (e^2 / 4a^4)[0.226Z(Z + 12f_m(r)) - B_1 + (A_2 - 5B_2) / 4 + 9.3204zaf'_m(r)]; \quad (\text{A.2})$$

$$C_{44} = (e^2 / 4a^4)[2.556Z(Z + 12f_m(r)) - B_1 + (A_2 + 3B_2) / 4]. \quad (\text{A.3})$$

The pressure derivatives of bulk modulus have been computed, whose expressions are as follows:

$$\frac{dB}{dp} = -(3\Omega)^{-1} \left[13.980Z(Z + 12f_m(r)) + C_1 - 3A_1 + C_2 - 3A_2 - \right. \\ \left. - 167.7648zaf'_m(r) + 41.9420za^2f_m(r) \right]; \quad (\text{A.4})$$

$$\Omega = -2.330Z(Z + 12f_m(r)) + A_1 + A_2 + 21.9612zaf'_m(r). \quad (\text{A.5})$$

The values of A_i , B_i , and C_i ($i = 1, 2$) have been evaluated from the knowledge of b , ρ and vdW coefficients. These parameters are defined as follows:

$$A_1 = L \left[\frac{d^2\phi_{ij}^{SR}(r)}{dr^2} \right]_{r=r}; \quad (\text{A.6})$$

$$B_1 = \left[-\frac{L}{r} \frac{d\phi_{ij}^{SR}(r)}{dr} \right]_{r=r}; \quad (\text{A.7})$$

$$A_2 = L \left[\frac{d^2\phi_{ii}^{SR}(r)}{dr^2} + \frac{d^2\phi_{jj}^{SR}(r)}{dr^2} \right]_{r=kr}; \quad (\text{A.8})$$

$$B_2 = -\frac{L}{r} \left[\frac{d\phi_{ii}^{SR}(r)}{dr} + \frac{d\phi_{jj}^{SR}(r)}{dr} \right]_{r=kr}; \quad (\text{A.9})$$

$$C_i = \frac{A_i^2}{B_i}, \quad (\text{A.10})$$

where, SR potential energies are

$$\phi_{ij}^{SR}(r) = b\beta_{ij} \exp\left(\frac{r_i + r_j - r}{\rho}\right) - \frac{C_{ij}}{r^6} - \frac{D_{ij}}{r^8}; \quad (\text{A.11})$$

$$\phi_{ii}^{SR}(r) = b\beta_{ii} \exp\left(\frac{2r_i - kr}{\rho}\right) - \frac{C_{ii}}{r^6} - \frac{D_{ii}}{r^8}; \quad (\text{A.12})$$

$$\phi_{jj}^{SR}(r) = b\beta_{jj} \exp\left(\frac{2r_j - kr}{\rho}\right) - \frac{C_{jj}}{r^6} - \frac{D_{jj}}{r^8}, \quad (\text{A.13})$$

where, $L = 2V/e^2$ (V/e^2) for NaCl (CsCl) structures, respectively, here, $V = 2r^3$ ($1.54r^3$) is the unit cell volume for NaCl (CsCl) structure, e is the amount of electronic charge.

Досліджено структурні, механічні та теплові властивості тугоплавких карбідів з використанням моделі дійсного інтерактивного потенціального наближення. Дослідження було поширено на змішані кристали сплавів $\text{Hf}_x\text{Ta}_{1-x}\text{C}$ ($0 \leq x \leq 1$) і $\text{Zr}_x\text{Nb}_{1-x}\text{C}$ ($0 \leq x \leq 1$), досліджено вплив складу на структурні і пружні властивості. Тиск фази переходу і пов'язані з ним об'ємні колапси ($\Delta V(P_i)/V(0)$), розраховані за такого підходу, добре узгоджуються з наявними в літературі для вихідних сполук ($x = 0$ і $x = 1$). Результати для змішаного кристалу протилежних частин також задовільно узгоджуються з експериментальними даними, отриманими на основі застосування закону Вегарда до даних вихідних сполук.

Ключові слова: сплав, кристалічна структура, фазові переходи, високий тиск, пружні властивості.

Исследованы структурные, механические и тепловые свойства тугоплавких карбидов с использованием модели действительного интерактивного потенциального приближения. Исследование было распространено на смешанные кристаллы сплавов $\text{Hf}_x\text{Ta}_{1-x}\text{C}$ ($0 \leq x \leq 1$) и $\text{Zr}_x\text{Nb}_{1-x}\text{C}$ ($0 \leq x \leq 1$), исследовано влияние состава на структурные и упругие свойства. Давление фазы перехода и связанные с ним объемные коллапсы ($\Delta V(P_i)/V(0)$), рассчитанные из такого подхода, хорошо согласуются с имеющейся в литературе данными для исходных соединений ($x = 0$ и $x = 1$). Результаты для смешанного кристалла противоположных частей также удовлетворительно согласуются с экспериментальными данными, полученными на основе применения закона Вегарда к данным для исходных соединений.

Ключевые слова: сплав, кристаллическая структура, фазовые переходы, высокое давление, упругие свойства.

1. Li J., Liao D., Yip S. et al. Force-based many-body interatomic potential for ZrC // J. Appl. Phys. – 2003. – **93**, N 11. – P. 9072–9085.
2. Dubrovinskaia N. A., Dubrovinsky L. S., Saxena S. K. et al. High-pressure study of titanium carbide // J. Alloys Comp. – 1999. – **289**, N 1–2. – P. 24–27.
3. Jun Z., Bo Z., Ying Q. J. et al. Thermodynamic properties of cubic ZrC under high pressure from first-principles calculations // Sci. China Press. – 2009. – **52**, N 7. – P. 1039–1042.
4. Wolf W., Podlucky R., Antrette T., Fische D. First-principles study of elastic and thermal properties of refractory carbides and nitrides // Philos. Mag. – 1999. – **79**, N 6. – P. 839–858.
5. Jun C. K., Shaffer P. T. B. Thermal expansion of niobium carbide, hafnium carbide and tantalum carbide at high temperatures // J. Less-Common Metals. – 1971. – **4**, N 3. – P. 323–327.
6. Kádas K., Andersson M., Holmström E. et al. Structural properties of amorphous metal carbides: Theory and experiment // Acta Mater. – 2012. – **60**. – P. 4720–4728.
7. Lawson A. C., Butt D. P., Richardson J. W., Li Ju. Thermal expansion and atomic vibrations of zirconium carbide to 1600 K // Philos. Mag. – 2007. – **87**, N 17. – P. 2507–2519.
8. Isaev I. E., Simak S. I., Brikosov I. A. et al. Phonon related properties of transition metals, their carbides, and nitrides: A first-principles study // J. Appl. Phys. – 2007. – **101**, N 12. – P. 123519–123537.
9. Ihara H., Hirabayashi M., Nakagawa H. Electronic band structures and x-ray photoelectron spectra of ZrC, HfC, and TaC // Phys. Rev. B. – 1976. – **14**, N 4. – P. 1707–1714.

10. *Smith H. G., Gläser W.* Phonon spectra in TaC and HfC // *Phys. Rev. Lett.* – 1970. – **25**, N 23. – P. 1611–1613.
11. *Liermann H. P., Singh A. K., Manoun B. et al.* Comparison behaviour of TaC_{0.98} under non-hydrostatic and quasi hydrostatic pressure upto 76 GPa // *Int. J. Refract. Met. Hard Mater.* – 2005. – **23**, N 5. – P. 109–114.
12. *Liermann H. P., Singh A. K., Somayazulu M., Saxena S. K.* Compression behavior of NbC under nonhydrostatic conditions to 57 GPa // *Ibid.* – 2007. – **25**, N 5–6. – P. 386–391.
13. *Acchar W., Segadaes A. M.* Properties of sintered alumina reinforced with niobium carbide // *Ibid.* – 2009. – **27**, N 2. – P. 427–430.
14. *Ramqvist L.* Electronic structure of cubic refractory carbides // *J. Appl. Phys.* – 1971. – **42**, N 5. – P. 2113–2120.
15. *Ivashchenko V. I., Turchi P. E. A., Shevchenko V. I.* Phase transformation B1 to B2 in TiC, TiN, ZrC and ZrN under pressure // *Condensed Matter Phys.* – 2013. – **16**, N 3. – P. 33602–33611.
16. *Amriou T., Bouhafs B., Aourag H. et al.* FP-LAPW investigations of electronic structure and bonding mechanism of NbC and NbN compounds // *Physica B.* – 2003. – **325**. – P. 46–56.
17. *Vanderbilt D.* Soft self-consistent pseudopotentials in a generalized eigenvalue formalism // *Phys. Rev. B.* – 1990. – **41**, N 11. – P. 7892–7895.
18. *Shrivastava A., Chauhan M., Singh R. K.* High-pressure phase transitions in transition metal carbides XC (X = Ti, Zr, Hf, V, Nb, Ta): a first-principle study // *Phase Transit.* – 2011. – **84**, N 1. – P. 58–66.
19. *Andrievskii R. A., Strel'nikova N. S., Poltoratskii N. I. et al.* Introduction and background on transition metal carbides // *Porosh. Met.* – 1967. – **7**, N 2. – P. 85–91.
20. *Zaoui A., Bouhafs B., Ruterana P.* First-principles calculations on the electronic structure of TiC_xN_{1-x}, Zr_xNb_{1-x}C and HfC_xN_{1-x} alloys // *Mat. Chem. Phys.* – 2005. – **91**, N 1. – P. 108–115.
21. *Farkas D. M., Groza J. R., Mukhejee A. K.* Thermodynamic analysis of carbide precipitates in a niobium-zirconium-carbon alloy // *Scripta Mater.* – 1996. – **4**, N 1. – P. 103–110.
22. *Sun Xiao-Wei, Zhang Xin-Yu, Zhang Su-Hong. et al.* // *Chinese Phys. B.* – 2013. – **22**, N 10, art. 107105.
23. *Singh R. K.* Many body interactions in binary ionic solids // *Phys. Rep.* – 1982. – **85**, N 5. – P. 259–401.
24. *Hafemeister W., Flygare W. H.* Outer-shell overlap integrals as a function of distance for halogen–halogen, halogen–alkali, and alkali–alkali ions in the alkali halide lattices // *J. Chem. Phys.* – 1965. – **43**, N 3. – P. 795–780.
25. *Slater J. C., Kirkwood J. G.* The van der Waals forces in gases // *Phys. Rev.* – 1931. – **37**, N 6. – P. 682–697.
26. *Tosi M. P.* Cohesion of ionic solids in the Born model // *Solid State Phys.* – 1964. – **16**, N 29. – P. – 1–120.
27. *Bhardwaj P., Sarwan M., Dubey R., Singh S.* Crystal structure and mechanical properties of actinide pnictides // *J. Mol. Struct.* – 2013. – **1043**, N 5. – P. 85–90.
28. *Bhardwaj P., Singh S.* Study of structural properties of partially covalent lanthanide and actinide bismuthides with phase transition pressures under 14 GPa // *Phys. Status Solidi (b).* – 2012. – **249**, N 1. – P. 38–49; Structural phase stability and elastic properties of refractory carbides // *Int. J. Refract. Met. Hard Mater.* – 2012. – **35**, N 1. – P. 115–121.
29. *Bhardwaj P., Singh S.* Temperature behaviour of narrow-gap semiconductors including galena // *Current Appl. Phys.* – 2014. – **14**, N 1. – P. 496–507.
30. *Vegard L.* Die Konstitution der Mischkristalle und die Raumfüllung der Atome // *Zeitschrift für Physik.* – 1921. – **5**, N 1. – S. 17–26.
31. *Singh A., Anayas M., Sanyal S. P.* High pressure behavior and structural properties of transition metal carbides // *Phase Transit.* – 2009. – **82**, N 8. – P. 576–586; Phase transition and high pressure behavior of zirconium and niobium carbides // *Cent. Eur. J. Phys.* – 2009. – **7**, N 1. – P. 102–107.
32. *Nartowski A. M., Parkin I. P., MacKenzie M. et al.* Solid state metathesis routes to transition metal carbides // *J. Mater. Chem.* – 1999. – **9**, N 6. – P. 1275–1281.
33. *Lierman H. P., Singh A. K., Manoun B. et al.* Compression behavior of TaC_{0.98} under nonhydrostatic and quasi-hydrostatic pressures up to 76 GPa // *Int. J. Refract. Met. Hard Mater.* – 2005. – **23**. – P. 109–114.
34. *Weber W.* Lattice dynamics of transition-metal carbides // *Phys. Rev. B.* – 1973. – **8**, N 11. – P. 5082–5092.

Received 08.04.15